Preprints (www.preprints.org) | NOT PEER-REVIEWED | Posted: 10 February 2017 doi:10.20944/preprints201702.0033.v1

Peer-reviewed version available at Batteries 2017, 3, , 14; doi:10.3390/batteries3020014

Article

Experimental Analysis of Thermal Runaway in 18650 Cylindrical Li-Ion Cells Using an Accelerating Rate Calorimeter

Boxia Lei [1], Wenjiao Zhao [1*], Carlos Ziebert [1], Nils Uhlmann [1], Magnus Rohde [1], and Hans Jürgen Seifert [1,]

[1] Institute of Applied Materials - Applied Materials Physics, Karlsruhe Institute of Technology, Germany
* Correspondence: wenjiao.zhao@kit.edu; Tel.: +49-721-608-28555

Abstract: In this work commercial 18650 lithium-ion cells with $LiMn_2O_4$, $LiFePO_4$ and $Li(Ni_{0.33}Mn_{0.33}Co_{0.33})O_2$ cathodes were exposed to external heating in an Accelerating Rate Calorimeter (es-ARC, THT Company) to investigate the thermal behavior under abuse conditions. New procedures for measuring external and internal pressure change of cells were developed. The external pressure was measured utilizing a gas-tight cylinder inside the calorimeter chamber in order to detect venting of the cells. For internal pressure measurements, a pressure line connected to a pressure transducer was directly inserted into the cell. During the thermal runaway experiments, three stages (low rate, medium rate and high rate reaction) have been observed. Both pressure and temperature change indicated different stages of exothermic reactions, which produced gases or/and heat. The onset temperature of thermal runaway was estimated according to temperature and pressure changes. Moreover, the different activation energies for the exothermic reactions could be derived from Arrhenius plots.

Keywords: Li-ion cell; Thermal runaway; Accelerating rate calorimeter (ARC); Pressure Change

1. Introduction

To get rid of the dependence of petroleum and to reduce the CO_2 emission, the best near-term solutions for vehicles probably are electric (EV) and hybrid electric vehicles (HEV). However, for their extensive market penetration one of the most urgent requirements is to develop lithium-ion cells and batteries, which are safe and reliable even at higher temperatures. Several exothermic chemical reactions can occur inside a cell while the temperature rises. This may generate heat that accumulates inside the cell and accelerates the chemical reaction between the cell components, if the heat transfer to the surroundings is not sufficient. In this case, a thermal runaway can occur in consequence with leak, smoke, gas venting, flames etc., which leads to fire or explosion.

To describe the thermal runaway the main exothermic chemical reactions have to be identified. According to [1-3] the thermal runaway process can be described by four main steps:

1) At $T > T_1$ the solid-electrolyte interface (SEI) decomposes in an exothermic reaction.
2) At $T > T_2$ an exothermic reaction between the intercalated Li-ions and the electrolyte starts.
3) At $T > T_3$ an exothermic reaction between the positive material and the electrolyte takes place with the evolution of oxygen inside the cell.
4) At $T > T_4$ the electrolyte decomposes.

A literature overview is given in Table 1. Abraham et al. [3] presented ARC measurements on 18650 lithium-ion cells to decipher the sequence of events leading to thermal runaway. At 84°C self-heating of the cell started. The gases generated in the cell were analyzed by gas chromatography/mass spectroscopy (GC/MS). Jhu et al. [4, 5], Chen et al. [6] and Lu et al. [8] studied

Preprints (www.preprints.org) | NOT PEER-REVIEWED | Posted: 10 February 2017 doi:10.20944/preprints201702.0033.v1

Peer-reviewed version available at Batteries 2017, 3, , 14; doi:10.3390/batteries3020014

thermal runaway characteristics (initial exothermic temperature, self-heating rate, pressure rise rate, maximum temperature and pressure) of Li-ion cells with different SOCs with vent sizing package 2(VSP2). The cathode materials of their tested commercial batteries were $LiCoO_2$, $Li(Ni_{1/3}Co_{1/3}Mn_{1/3})O_2$ and $LiFePO_4$. For all cathode materials, high SOC levels aggravated the exothermic reactions. They also compared the self-heating behaviors of cells with different voltages by the heat of reaction (ΔH), which was the product of mass of a cell, specific heat capacity of the cell and the rise of temperature under adiabatic conditions [4-6,8]. In addition, the activation energy as well as the frequency factor were calculated with the Arrhenius equation. Fleischhammer et al. [7] showed the differences in the safety behavior between un-aged and aged 18650 Li-ion cells by ARC. The cells that were cycled at low temperature were proven to be the most hazardous one, in comparison to the un-aged cells and cells cycled at high current. Hence, lithium plating leads to a significant increase of heat formation and the ageing history has a strong influence on the safety of the cells. Mendoza-Hernandez et al. [9] used ARC to study the thermal runaway behavior of $LiCoO_2$ and $LiMn_2O_4$ cathode materials at different SOCs. The cell with $LiMn_2O_4$ cathode material was found to be more thermally stable than the cell with $LiCoO_2$. In a recent SANDIA report [10] the effects of cell size on thermal runaway energetics of the cylindrical cells from 3 to 50 Ah of both $LiFePO_4$ (LFP) and $LiNi_{0.80}Co_{0.15}Al_{0.05}O_2$ (NCA) chemistries were studied. Results show that for both LFP and NCA cells, the normalized heating rate (W/Ah) increases roughly linearly for cells from 3-38 Ah while the normalized total heat released (kJ/Ah) is relatively constant over that cell size range. Selman et al. [11] used also ARC to study the thermal runaway behavior of $LiCoO_2$ cathode materials at different voltages. The fully charged Li-ion cell had the lowest onset self-heating temperature.

Golubkov et al. [12] ran thermal runaway tests on batteries of $LiFePO_4$ (LFP), $Li(Ni_{0.45}Mn_{0.45}Co_{0.10})O_2$ (NMC) and blended LCO/NMC cathode materials by using a pressure-tight and airtight reactor, which was able to collect gases. CO, CO_2 and H_2 represented about 80% of the produced gases, and the others were CH_4 and C_2H_4. The onset temperatures and released gas amounts of LFP, NMC and LCO/NMC were 195 °C and 50 mmol, 170 °C and 150 mmol, 150 °C and 270 mmol, respectively.

In this work, four kinds of experimental methods were applied to measure the surface temperature of the tested commercial 18650 cells, the pressure change due to released gases and the pressure change in re-sealed cells. The correlation between pressure and temperature behavior of lithium ion cells can characterize the degree of violence of a thermal runaway [4], and is very helpful in defining the threshold, the stages of thermal runaway, and the different reactions during thermal runaway.

2. Experimental

For commercial 18650 lithium-ion cells with $LiMn_2O_4$ (LMO), $LiFePO_4$ (LFP) and $Li(Ni_{0.33}Mn_{0.33}Co_{0.33})O_2$ (NMC) cathodes, four different thermal runaway testing methods have been applied in an accelerating rate calorimeter (es-ARC, THT Company). The calorimeter chamber with a diameter of 10 cm and a height of 10 cm has one heater and one thermocouple located in the lid and in the bottom; and two heaters and thermocouples (all type N) in the side wall. The tested cell is fixed on the lid of the calorimeter as shown in Figure 1. The calorimeter temperature is controlled by a main or so-called bomb thermocouple attached onto the surface of the cell. The heaters work until reaching the required temperatures regarding the measurement conditions and modes. A steel casing outside serves as a protection.

2.1 First Method(Only Temperature Measurement OT)

In the first method, only temperature and temperature rate were recorded (Figure 1 (a)). The standard Heat-Wait-Seek (HWS) method was applied for all measurements. The procedure and the

Table 1

Literature overview on accelerating rate calorimetry measurements of thermal runaway behavior by cylindrical lithium-ion cells

Author	Cell Type					Calori-meter Type	SOC in % or voltage in V	Onset temperature of self-heating in °C	Maximum temperature T_{max} in °C	Heat of reaction ΔH in kJ	T_{Vent} in °C	Maximum pressure P_{max} in bar
	Manufacturer/ Name	Capacity in Ah	Dimensions	Weight in g	Materials (cathode/ anode)							
Abraham [3]	Quallion LLC	1	Cylindrical 18650	-	NCA/ graphite	ARC	100	84	-	-	124	-
Jhu [4]	-	2.6	Cylindrical 18650	44.9	LCO/ -	VSP2	100	131.5	708.8	18.9	-	18.6
	-	2.0	Cylindrical 18650	41.7	NMC/ -		100	175.4	665.6	14.9	-	11.3
Jhu [5]	Sanyo/ UR18650F	2.6	Cylindrical 18650	45.5	LCO/ -	VSP2	4.2	131.3	708.7	19.2	-	13.5
							3.7	172.8	402.6	7.7		3.6
	Sony/ SE US18650GR			44.5			4.2	125.2	654.3	17.9	-	24.5
							3.7	154.8	517.2	12.3		3.1
	Samsung/ ICR 18650-26D			44.8			4.2	116.5	683.2	18.6	-	18.1
							3.7	152.8	454.8	10.2		4.0
	LG/ LGDB218650			46.5			4.2	142.5	691.9	18.4	-	15.8
							3.7	168.0	407.1	8.0		3.3
Chen [6]	Sony/ SE US18650GR	2.6	Cylindricalal 18650	46.5	LCO/ graphite	VSP2	0	-	-	-	200	-
							30	175	241	2.5	175	2.9
							50	174	441	10.2	175	4.0
							80	140	638	19.0	175	5.9
							100	122	660	20.6	160	16
Fleisch-hammer [7]	-	1.5	Cylindrical 18650	-	NCM/LMO carbon/ graphite	ARC	Un-aged High-rate aged Low temp. aged	97.9 80.5 42.1	-	-	-	-
Lu [8]	-		Cylindrical 18650	38.15 32.84 44.8 44.89	LFP/- LCO/-	VSP2	3.3 3.6 3.7 4.2	200.5 199.94 160.45 130.54	217.75 243.23 280.10 370.03	0.47 1.02 3.91 7.85	-	17.2 17.89 34.34 116.44
Mendoza-Hernandez [9]	-	0.8	Cylindrical 18650	-	LCO/ graphite	ARC	0 25 50	165.3 159.8 155.1	-	-	-	-

Preprints (www.preprints.org) | NOT PEER-REVIEWED | Posted: 10 February 2017 doi:10.20944/preprints201702.0033.v1

Peer-reviewed version available at Batteries 2017, 3, , 14; doi:10.3390/batteries3020014

	-	0.72	Cylindrical 18650	-	LMO/ graphite		75 100 120 0 25 50 75 100 120	140.1 124.9 116.5 - 109.9 104.9 104.9 104.9 99.8	-	-	-	-
Orendorff [10]	-	2.6 3.4 20 27 30 38	Cylindrical	-	LFP NCA LFP NCA LFP LFP	ARC BTPV[1]		175 160 235 110 250 233-246	-	19.4 31.1 150 254 272 289	-	0.16 0.45 1.3 4.1 - 1.8
Selman [11]	Sony		Cylindrical 18650	-	LCO/ carbon	ARC	2.8 4.06	144 104	-	-	-	-
this work		1.65 1.1 2.2	Cylindrical 18650	43.4 39.7 41.7	LMO LFP NMC	ARC	100	91 90 91	303 259 731	7.8 7.3 24.9	-	

[1] BTPV: Battery Testing Pressure Vessel

Preprints (www.preprints.org) | NOT PEER-REVIEWED | Posted: 10 February 2017 doi:10.20944/preprints201702.0033.v1

Peer-reviewed version available at Batteries 2017, 3, , 14; doi:10.3390/batteries3020014

Preprints (www.preprints.org) | NOT PEER-REVIEWED | Posted: 10 February 2017 doi:10.20944/preprints201702.0033.v1

Peer-reviewed version available at Batteries 2017, 3, , 14; doi:10.3390/batteries3020014

data recording are shown in Figure 2 and Figure 3 respectively. The HWS method starts at 25 °C in the Heat Mode by heating up the cell in small temperature steps of 5° C (see Figure 3). At the end of each temperature step the Wait Mode is activated for 15 min to reach thermal equilibrium. After reaching thermal equilibrium, the system enters Seek Mode, which monitors the temperature rate and ends up with two possible modes—Exotherm Mode or Heat Mode. The decision is related to the selected Temperature Rate Sensitivity. If the measured temperature rate is larger than this value, the system goes into Exotherm Mode. This mode provides an adiabatic environment, which means that no heat exchange between the sample and the surrounding exists, so that the heat energy of reactions can be monitored by the measured temperature. On the other hand, if the temperature rate is smaller, the system goes back into Heat Mode. If the temperature exceeds the given final temperature T_f(250 °C), the heaters shut down totally and it will be cooling down by introducing pressurized air to the calorimeter chamber.

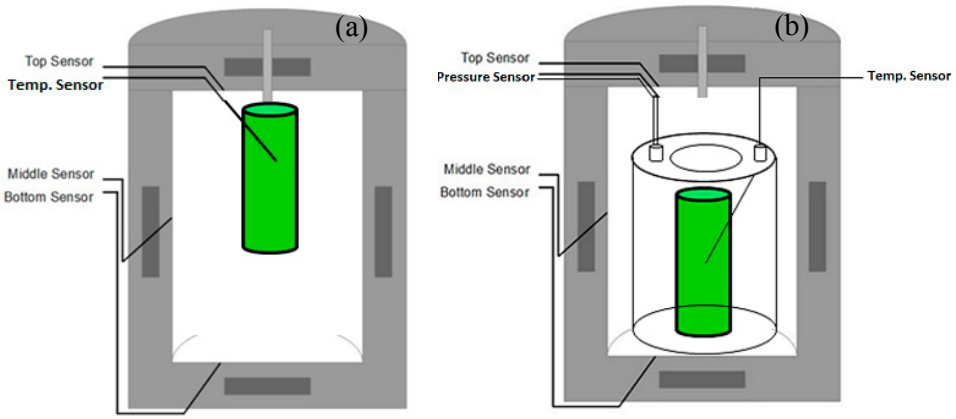

Figure 1. Setup of the cell in the ARC: (a) Normal and internal pressure measurement (b) External pressure measurement.

2.2 Second Method(External Pressure Measurement EP)

For the second method, an additional cylinder chamber was used in external pressure measurements (see Figure 1 (b)). The thermocouple was introduced through a well-sealed hole and a pressure line connected with a pressure sensor was screwed on the cylinder chamber. It was very critical to screw every part of the cylinder chamber extremely tight to prevent leaks. Similar to the adiabatic environment, it's capable to monitor the external pressure change only if under the air-tight condition.

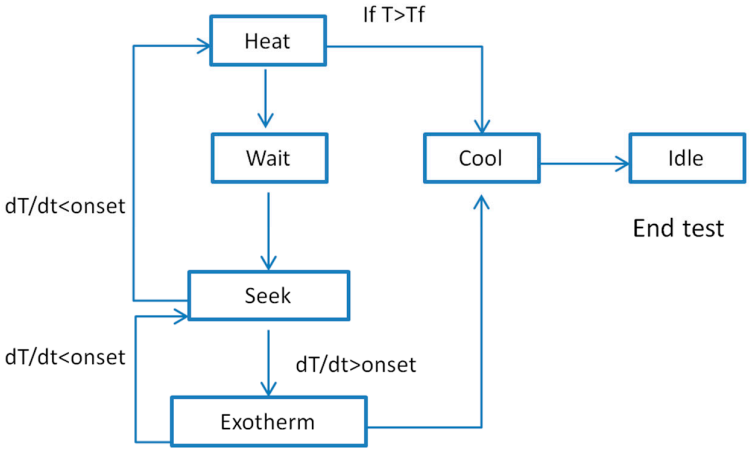

Figure 2. Process of heat-wait-seek (HWS) method.

Preprints (www.preprints.org) | NOT PEER-REVIEWED | Posted: 10 February 2017 doi:10.20944/preprints201702.0033.v1

Peer-reviewed version available at Batteries 2017, 3, , 14; doi:10.3390/batteries3020014

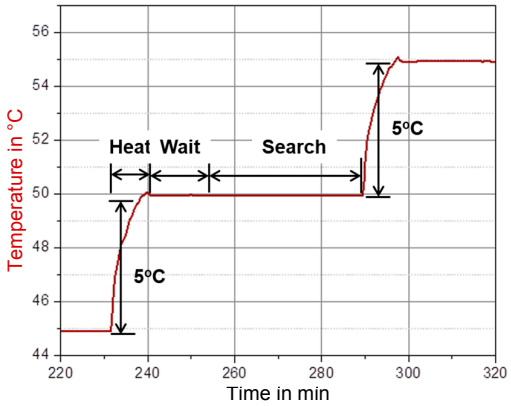

Figure 3. Example of temperature data recording.

2.3 Third Method (Internal Pressure Measurement IP)

In contrast to the set-up of the second method, where the capillary leading to the pressure sensor was connected to the cylinder, in the third method the capillary was directly introduced into the functional cell for internal pressure measurements (Figure 4). Therefore, a suitable point, which can let the capillary go through without disturbing the functionality of the cell, had to be found with the help of X-ray tomography images.

X-ray tomography was conducted in the IAM X-Ray Imaging Laboratory at KIT. X-ray micro-tomography scans were performed on the cell using a Phoenix v/tome/x s system (Phoenix X-ray, GE Measurement and Control, Germany). The battery was rotated 360° around its long axis whilst 1600 projections were captured with the microfocus tube operating at 200 kV and 370(230) µA. The sample and detector were positioned in projection magnification providing an effective voxel size of 75(48) µm for the high resolution imaging. Tomography scans of the full cell were obtained, and subsequent 3D analysis of the reconstructed image data was performed using VG studio max software (Volume Graphics Company, Germany). For instance, Figure 4 shows a 3D rendering of the tomographic data set for the 18650 cell with LMO cathode. The spirally layer structure of the cell and the hollow central section are clearly revealed as well as the safety valve on the top. It was easy to draw the conclusion that the best position for the pressure line is located on the bottom center. The reasons are

1. The hollow is big enough for inserting a 1/16-inch diameter capillary.
2. Inside the battery, the hollow section is located exactly in center; nothing will be damaged for drilling a hole.

Then the cells have been resealed with epoxy resin. The described preparation procedure was conducted in an Argon-filled glovebox, because the cell components are very sensitive to moisture and oxygen.

2.4 Fourth Method (Ramp Heating Method (Hotbox test))

For the 'Ramp Heating' method the cells have been set up in the same way as described before for the HWS tests. However, instead of a stepwise heating of the cells, they were heated up continuously from 30°C to 250°C in the ARC at a constant rate of 5°C/min. This mimics a Hot Box test. For this purpose, the measurements were operated in 'Ramp Mode' with a high sensitivity value of 6°C/min to prevent the automatic switching into the 'Exotherm Mode'. The system was used under adiabatic conditions, as in the other tests.

Preprints (www.preprints.org) | NOT PEER-REVIEWED | Posted: 10 February 2017 doi:10.20944/preprints201702.0033.v1

Peer-reviewed version available at Batteries 2017, 3, , 14; doi:10.3390/batteries3020014

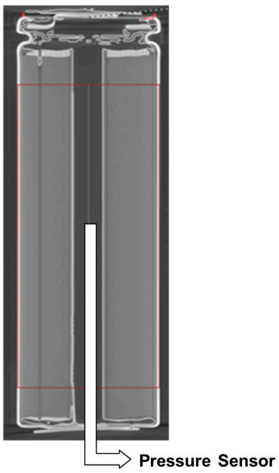

Figure 4. Setup for internal pressure measurement.

2.5 *Cells Preparation*

Before the thermal runaway tests, the capacity of the cells was determined by three full cycles and finally they were fully charged to state of charge 100% (SOC100), because this is the most critical condition for thermal runaway according to [7]. The method of charge was CC/CV. Which means that firstly the cell is charged at constant current at 1C rate (CC) till the maximal voltage, and then it is charged at constant voltage (CV) with decreasing current until the current reaches 10% of its starting value.

3. Results and Discussion

3.1. Results for 18650 cells with LMO cathode by using different methods

In the following the first three test methods are demonstrated exemplarily for the cell with LMO cathode in the temperature range of 25 to 250°C. Figure 5 compares the time evolution of the measured surface temperatures for the three different methods with three identical cells at SOC100. From this figure, it is easy to distinguish the Heat-Wait-Seek periods from the Exotherm periods. At temperatures below about 80°C, the temperature curve increased with steps of 5°C. Then a first exothermic reaction can be observed where the self-heating rate is higher than 0.02°C/min. Afterwards, the system went back to Heat Mode at 100°C, and the HWS Mode was active until 110 °C. Then the temperature went up continuously in Exotherm Mode until thermal runaway happened.

So three stages were observed in the thermal runaway tests, which were assigned according to the literature [1-3] to:

1) At about 80 °C the solid electrolyte interface (SEI) decomposed.
2) At about 110 °C an exothermic reaction between embedded Lithium ions and electrolyte started, which resulted in the reduction of electrolyte at the negative electrode.
3) At about 200 °C an exothermic reaction between active material and electrolyte at positive electrode took place.

When comparing the three curves, the time period in HWS Mode before switching into Exotherm Mode, increased from the only temperature via the external up to the internal pressure measurements. The reason is that for the external pressure tests, the system needs to heat up the cylinder and that for internal pressure tests, some heat loss occurs via the metallic pressure line. Even though the three curves do not perfectly overlap each another, the tendencies are the same. The

Preprints (www.preprints.org) | NOT PEER-REVIEWED | Posted: 10 February 2017 doi:10.20944/preprints201702.0033.v1

Peer-reviewed version available at Batteries 2017, 3, , 14; doi:10.3390/batteries3020014

Figure 6, which shows the temperature rate vs. the temperature, gives us a more specific view. From that the three stages can be distinguished more easily. In the temperature region from 80 °C to 150 °C, the temperature rate is lower than 1 °C/min. From 150 °C to 200 °C, the energy was released with a medium rate lower than 25 °C/min. Above 200 °C, the exothermic reactions happened in a violent way with a temperature rate over 1000 °C/min.

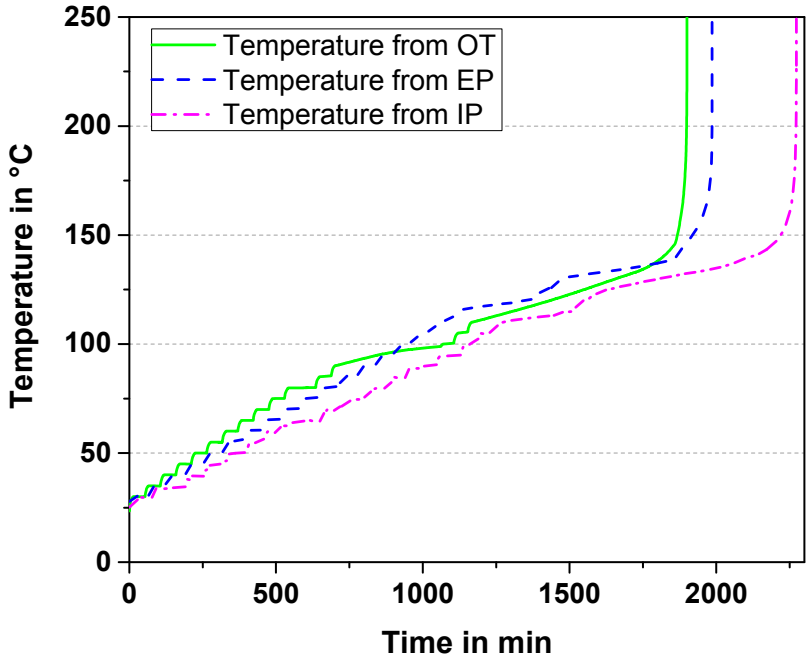

Figure 5. Comparison of temperature vs. time curves measured with different methods.

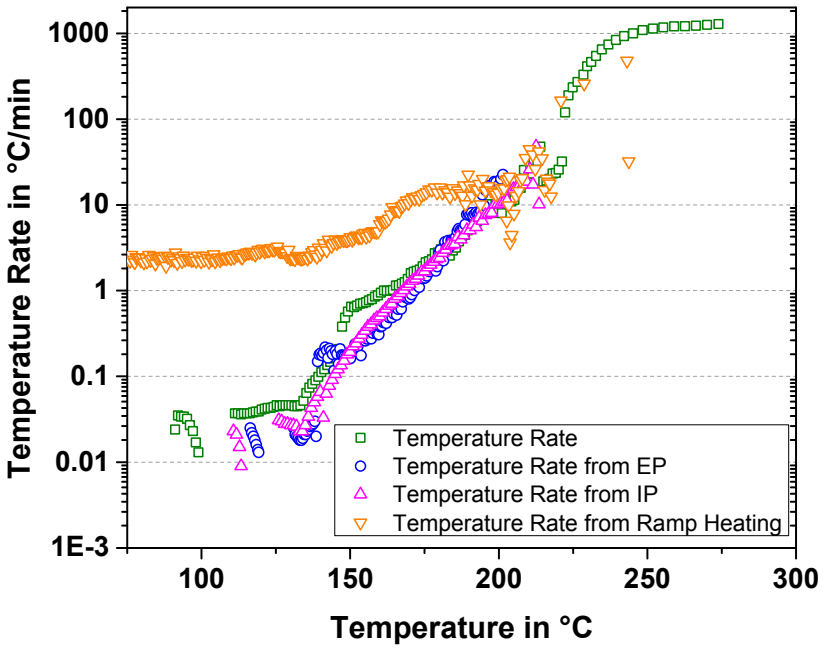

Figure 6. Comparison of temperature rate vs. temperature curves measured with different methods.

Preprints (www.preprints.org) | NOT PEER-REVIEWED | Posted: 10 February 2017 doi:10.20944/preprints201702.0033.v1

Peer-reviewed version available at Batteries 2017, 3, , 14; doi:10.3390/batteries3020014

In Fig. 7 the HWS method without pressure measurement (s. Fig.7a)) is compared to the ramp heating method (Fig. 7b)). From the latter, less information could be extracted: it can be seen that the temperature increased linearly at the beginning as shown in Figure 7b) and that the inflection point was at about 150 °C, which could also be observed in the curve of temperature rate vs. temperature (s. Fig. 6). Comparatively, the HWS Mode is relatively sensitive and able to tell the whole story about thermal runaway.

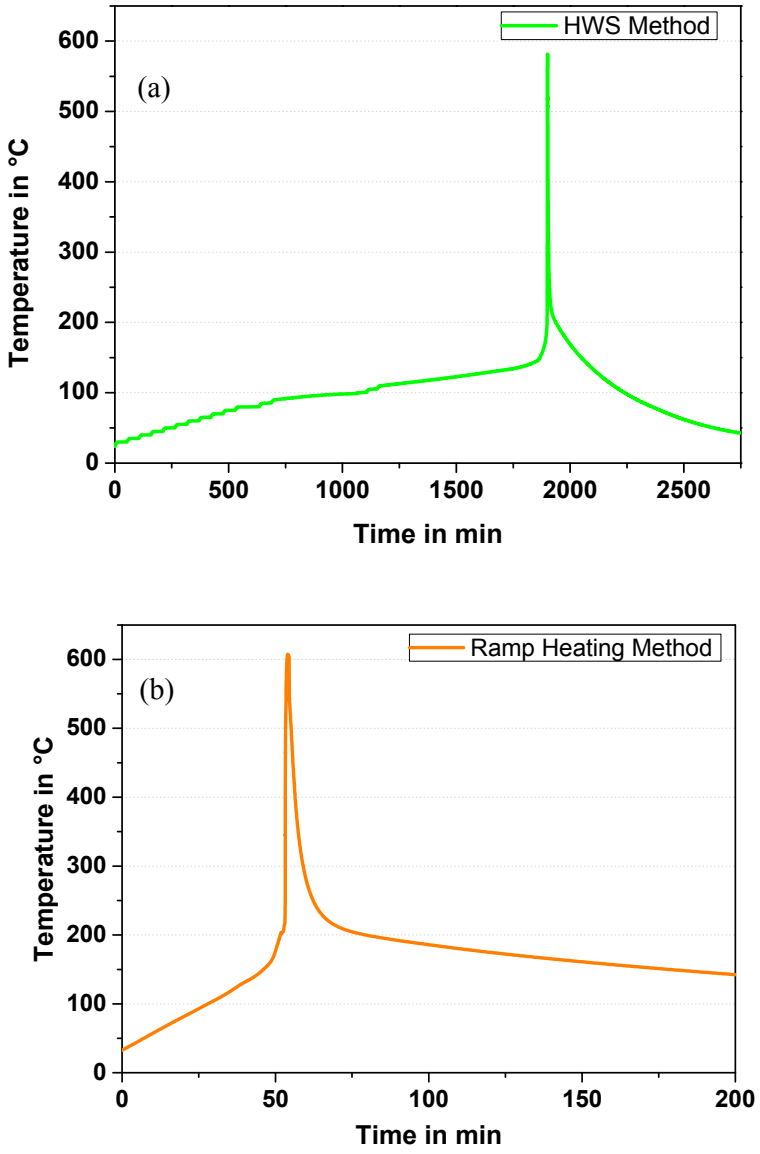

Figure 7. Comparison of temperature vs. time curves: (a) HWS Method, (b) Ramp Heating Method.

In Figure 8 the pressure vs. time curves for external and internal pressure tests are compared. In the external pressure curve (blue line) at about 130 °C a small pressure rise can be observed, which is the beginning of air leaking of the cell. At the end of stage 2, it could be deduced that the battery had opened and gases were released. The external pressure increased continuously and dramatically until 21 bar at stage 3, matching the temperature change very well. From the internal pressure curve (magenta line), we can see that the internal pressure was increasing steadily during stage 1 and 2. In the transition from stage 2 to 3, the cell vented and gases were released, which was indicated by a rapid internal pressure drop.

Preprints (www.preprints.org) | NOT PEER-REVIEWED | Posted: 10 February 2017 doi:10.20944/preprints201702.0033.v1

Peer-reviewed version available at Batteries 2017, 3, , 14; doi:10.3390/batteries3020014

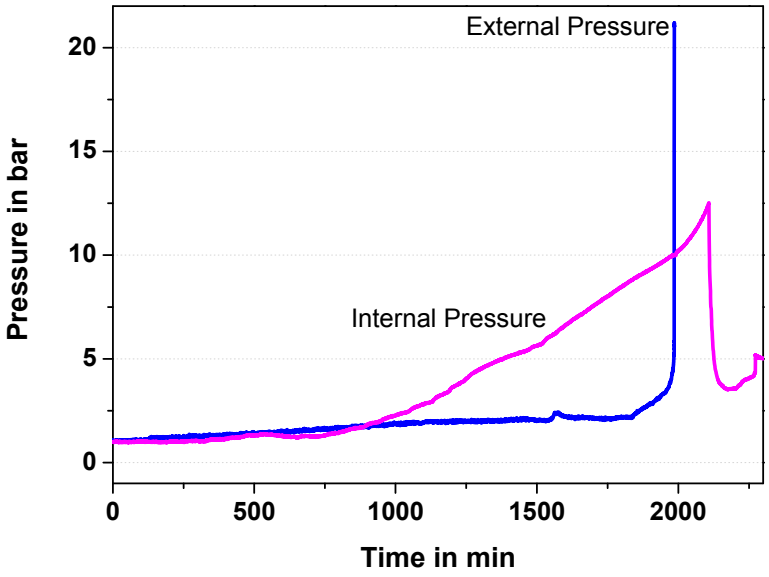

Figure 8. Comparison of pressure curves vs. time with different methods.

Finally in order to correlate temperature and pressure measurements, the pressure values measured from the external and the internal pressure tests are plotted vs. the temperature in Figure 9. For both external and internal pressure curves, the inflexion was at 130 °C, where the cells vented produced gases to reduce internal pressure. At the same time, it caused increasing of the external pressure.

The additional red line represents the expansion of the air with increasing temperature according to the ideal gas law. For the external pressure measurement, the difference between the measured blue line and the red line can be regarded as the amount of gases that come from the leaking cell. As the temperature increased, the difference became larger and larger, indicating that more and more gases were produced. There was a gas leaking from 80°C and produced gases were released into the cylinder, because of exceeding the threshold pressure of the safety valve. At 130 °C, the difference became larger. At 200 °C, which was also the start temperature point of stage 3, the difference was significant. For the internal pressure measurement, starting at 80 ° C, the difference was increasing continuously, indicating the beginning of gas production and SEI layer decomposition.

From ideal gas law, the following equation is derived:

$$n_0 = (p_0 \cdot V_0) / (R \cdot T_0), \quad (1)$$

$$n_1 = (p_1 \cdot V_0) / (R \cdot T_1), \quad (2)$$

where n_0 is the original air amount in the cylinder, p_0 is the pressure of original air, T_0 represents the temperature of original air, V_0 represents the volume of the cylinder,. and R is the gas constant, taken as 8.316 $J\,K^{-1}\,mol^{-1}$. Similarly, n_1 represents the actual gases amount measured during the measurements, p_1 is the pressure of actual gases, T_1 represents the temperature of actual gases. From the parameters, depth: 72mm, outer diameter: 82 mm and thickness: 5 mm, the volume is calculated: $2.73 \cdot 10^{-4} m^3$. At the beginning of the measurement, temperature and pressure in the cylinder were 27.83°C (300.98 K) and 1.11 bar ($1.11 \cdot 10^5$ Pa), which gives n_0 =12.05 mmol. At the end of the measurement, thermocouple and pressure sensor detected that the sample temperature was 35.0 °C (308.15 K) and the pressure in the cylinder was 8.31 bar ($8.31 \cdot 10^5$ Pa), calculating

Preprints (www.preprints.org) | NOT PEER-REVIEWED | Posted: 10 February 2017 doi:10.20944/preprints201702.0033.v1

Peer-reviewed version available at Batteries 2017, 3, , 14; doi:10.3390/batteries3020014

n_1= 88.53 mmol. Thus, the amount of produced gases during thermal runaway is (88.53-12.05) mmol, which is 76.48 mmol.

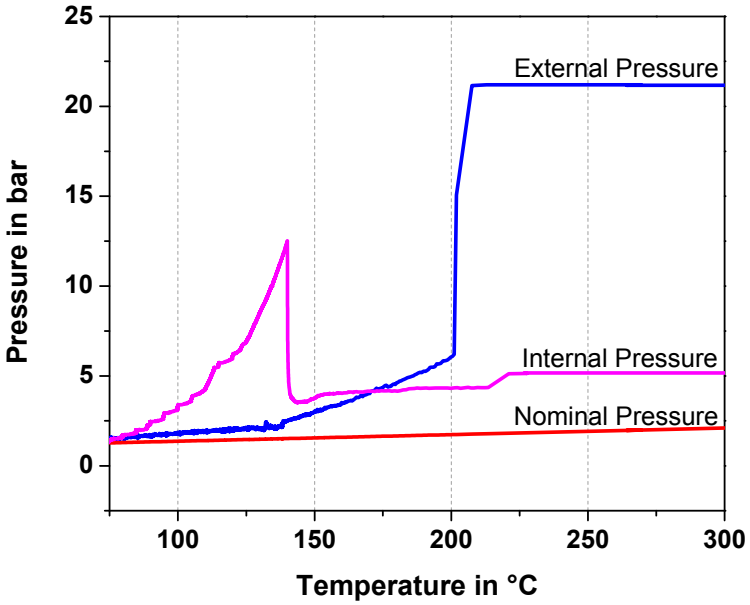

Figure 9. Comparison of pressure vs. temperature curves with different methods.

A similar procedure was described by Golubkov et al. [6] and the amount of produced gases was calculated from the measured external pressure. The cell with LMO cathode released 76.5 mmol gases during thermal runaway. Golubkov et al. reported that 18650 cells with LCO/NMC cathode material released gases of 265 mmol, and those with pure NMC 149 mmol. This comparison indicates a better exothermic stability of the LMO cathode.

3.2. Results for 18650 cells with different cathode materials

In the market, there are many kinds of batteries, varying from geometry to material. The most common structures of cathode materials are spinels, layered oxides and olivines. Not only their electrical performance but also their thermal properties are quite different. Thus, every kind of these three active materials should be investigated and compared in 'thermal runaway' studies [13]. The second part of this work focuses on comparison of their thermal behavior in cylindrical 18650 cells. Their specifications are listed in Table 2. LMO, LFP and NMC are chosen as examples for spinel, olivine and layered structure respectively in this work.

Table 2. Specifications of 18650 Li-Ion cells with different cathode materials.

Cathode Material	$LiMn_2O_4$ (LMO)	$LiFePO_4$ (LFP)	$Li(Ni_{0.33}Mn_{0.33}Co_{0.33})O_2$ (NMC)
U_{min}-U_{max} in V	2.5 - 4.2	2.0 - 3.6	2.75 - 4.2
Nominal Capacity in mAh	1650	1100	2200
Cycle Life	1000	>1000	>300
Weight in g	43.4	39.7	41.7
Operating temperature in °C	-20 to 60	-30 to 60	-20 to 60

Figure 10 shows the thermal behavior of 18650 cells during 'thermal runaway' measurements. In all tests the cells were heated between 30 and 250 °C with 5°C increments in the search for

Preprints (www.preprints.org) | NOT PEER-REVIEWED | Posted: 10 February 2017 doi:10.20944/preprints201702.0033.v1

Peer-reviewed version available at Batteries 2017, 3, , 14; doi:10.3390/batteries3020014

self-heating at the sensitivity threshold of 0.01° C/min. In the plot temperature vs. time, all of the onset temperatures of exothermal reactions were similar, at about 90 °C. The comparison of the maximum temperatures gives the highest value of 731 °C for the NMC cathode, while it's only 259 °C for the LFP cathode. One reason is the difference of the capacities, i.e. the nominal capacity of NMC (see Table 2.) is twice than that of LFP. Because the nominal capacity of LMO lies in between, its maximum temperature of LMO does the same with 303 °C. In terms of time consume for heating until exothermal reactions start, NMC and LFP took slightly longer than LMO.

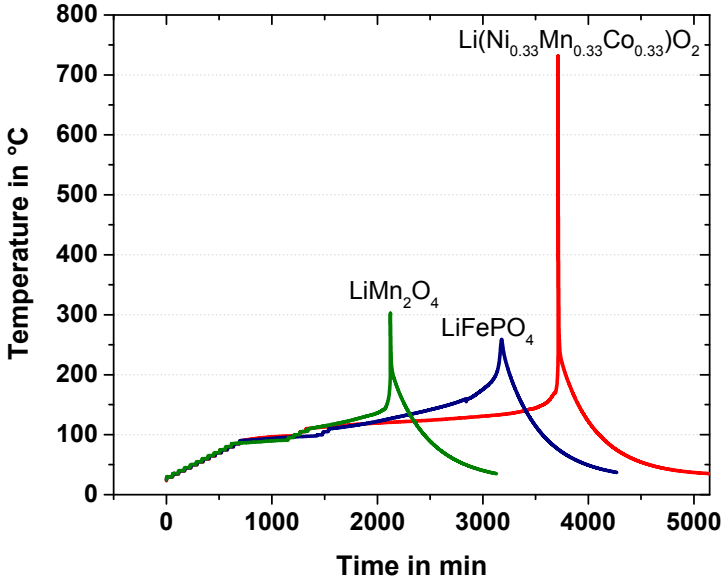

Figure 10. Temperature vs. time curves for 18650 cells with different cathode materials.

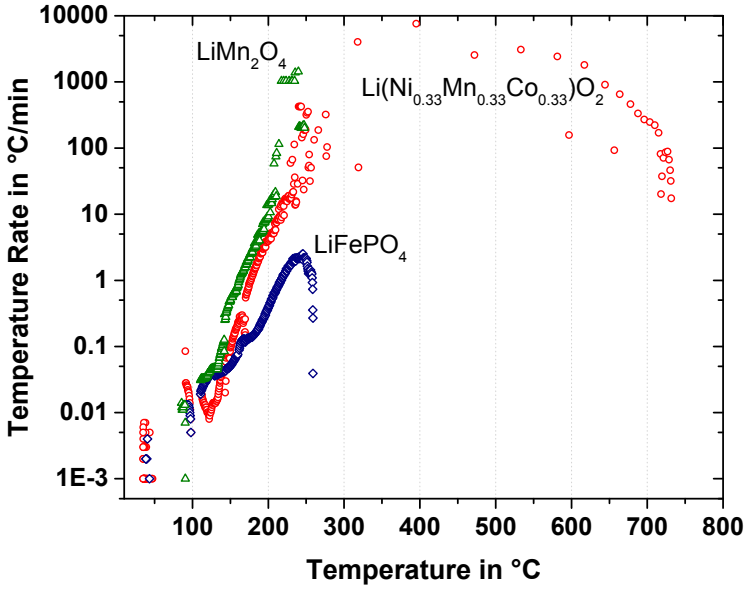

Figure 11. Temperature rate vs. temperature curves for 18650 cells with different cathode materials.

In the temperature rate vs. temperature plot shown in Figure 11, the three different stages of thermal runaway mentioned before could be observed and distinguished. The LFP cell had never entered stage 3 with temperature rates staying below 3 °C/min. On the contrast, the LMO cell reached a maximum rate of 1430 °C/min and the NMC cell even 7580 °C/min. In the temperature

Preprints (www.preprints.org) | NOT PEER-REVIEWED | Posted: 10 February 2017 doi:10.20944/preprints201702.0033.v1

Peer-reviewed version available at Batteries 2017, 3, , 14; doi:10.3390/batteries3020014

region between 80 °C to 130 °C, the solid electrolyte interface (SEI) decomposed. The temperature rate of LFP was the lowest among these three materials, while NMC and LMO were in the same range. The much lower maximum temperature rate of LFP can not only be attributed to the lower capacity but also to the much higher thermal stability of this nanoscale material.

According to the simplified equation for calculating the thermokinetic parameters proposed by Jhu et al. [4-6], which is based on the Arrhenius law, the temperature rate or self-heating rate can be expressed as follows:

$$\ln (dT/dt) \approx \ln (\Delta T_{ad} \cdot A) - E_a/(k_B \cdot T), \quad (3)$$

and the heat of reaction (J/g) for each stage can be calculated with the equation:

$$\Delta H/m_{cell} = c_p \cdot \Delta T_{ad}, \quad (4)$$

where A is pre-exponential factor (min^{-1}), ΔT_{ad} is the adiabatic temperature rise (K), i.e. the difference between the initial exothermic temperature T_0 and the maximum temperature T_{max}, E_a is the activation energy (eV), k_B is Boltzmann's constant (8.62e-5 eV· K^{-1}), m_{cell} is the cell mass (g), and c_p is the heat capacity (J/g·K). Thus, by plotting the natural logarithm of the self-heating rate versus the inverse of temperature as shown in Figure 12, the activation energy and frequency factor of the different cells can be calculated. The data obtained from this Arrhenius plot are listed in Table 3. Obviously Li-ion cells with LFP cathode have the lowest T_{max} and $(dT/dt)_{max}$, while cells with NMC cathode show the highest T_{max} and $(dT/dt)_{max}$. For calculating the heat of reaction using equation (2) the heat capacity was measured as described in Schuster et al. [15]. The listed heat of reaction is the sum of the heats of reaction of the different stages. The heats of reaction show a good agreement with results from literature [2, 14] and the activation energies as well [5]. The next step could be to use the derived thermokinetic parameters as input parameters for our coupled electrochemical thermal model [16]. This model is based on the porous electrode theory of Newman [17] and has been extended with a simple combustion model coming from reaction kinetics including various types of heat sources based on an Arrhenius law.

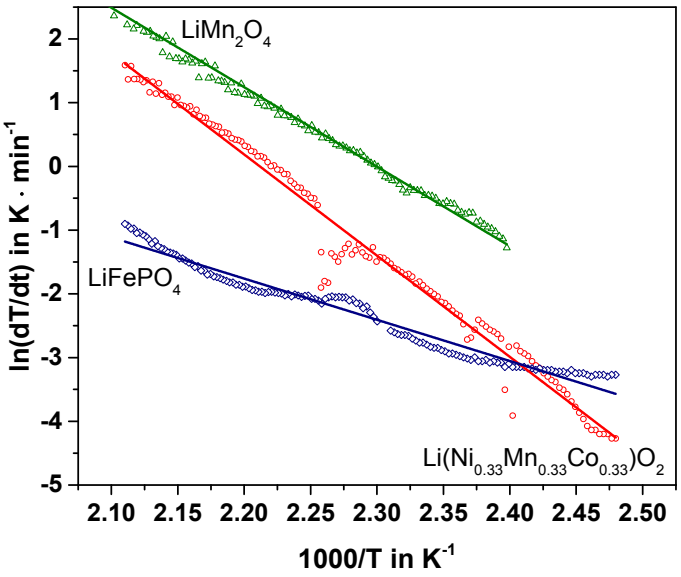

Figure 12. Natural logarithm of the self-heating rate vs. inverse of temperature curves for 18650 cells with different cathode materials.

Preprints (www.preprints.org) | NOT PEER-REVIEWED | Posted: 10 February 2017 doi:10.20944/preprints201702.0033.v1

Peer-reviewed version available at Batteries 2017, 3, , 14; doi:10.3390/batteries3020014

Table 3. Thermal runaway test results of 18650 Li-Ion cells with different cathode materials.

Cathode Material	$LiMn_2O_4$ (LMO)	$LiFePO_4$ (LFP)	$Li(Ni_{0.33}Mn_{0.33}Co_{0.33})O_2$ (NMC)
Onset temperature of self-heating in °C	91	90	91
T_{max} in °C	303	259	731
$(dT/dt)_{max}$ in °C/min	1429	3	7577
c_p at 60°C SOC100 in J/g·K	0.83	1.19	0.95
E_a in eV	1.07	0.56	1.37
Reaction heat in J/g	180	184	597
Reaction heat in J/g	350-640 [2,14]	260 [14]	600 [14]

4. Conclusions

Three stages have been observed in thermal runaway tests in 18650 Li-Ion cells with LMO cathode by correlating temperature and pressure curves. The first stage began with gases production at about 80 °C. The reaction in the first stage was likely to be the SEI layer decomposition. The onset temperature was about 113 °C, when the second stage started; from this temperature, the cells started self-heating until the thermal runaway. The amount of produced gases was 76.48 mmol in thermal runaway. In future studies, it could be interesting to confirm all these stages exactly and analyze produced gases and material components after thermal runaway using post-mortem analysis by opening the cells those were frozen at the different stages.

For 18650 Li-Ion cells with different cathode materials, the thermal runaway tests confirmed that cells with LFP cathode exhibited a good stability under thermal abuse, while cells with NMC cathode presented a poor temperature tolerance at high temperatures.

Acknowledgments: This R&D project is part of the project IKEBA which was funded by the German Federal Ministry for Education and Research (BMBF) within the framework "IKT 2020 Research for Innovations" under the grant 16N12515 and was supervised by the Project Management Agency VDI | VDE | IT. The authors would like to express their gratitude to A. Maier, IAM-AWP, for recording the X-Ray tomography images.

Author Contributions: Professor Hans Juergen Seifert inspired and conducted the fundamental idea of this work. Carlos Ziebert and Magnus Rohde conceived and designed the experiments; Wenjiao Zhao, Boxia Lei and Nils Uhlmann performed the experiments; Boxia Lei and Wenjiao Zhao analyzed the data.

Conflicts of Interest: The authors declare no conflict of interest. The funding agency had no role in the design of the study; in the collection, analysis, or interpretation of data; in the writing of the manuscript, and in the decision to publish the results.

References

1. E.P. Roth, D.H. Doughty, Thermal abuse performance of high-power 18650 Li-ion cells. J. Power Sources, 128, 308 (2004).
2. R. Spotnitz, J. Franklin, Abuse behavior of high-power, lithium-ion cells. J. Power Sources, 113, 81 (2003).
3. D.P. Abraham, E.P. Roth, R. Kostecki, K. McCarthy, S. MacLaren, D.H. Doughty. Diagnostic examination of thermally abused high-power lithium-ion cells. J. Power Sources, 161, 648 (2006).
4. C.-Y. Jhu, Y.-W. Wang, C.-Y. Wen, C.-M. Shu, Thermal runaway potential of $LiCoO_2$ and $Li(Ni_{1/3}Co_{1/3}Mn_{1/3})O_2$ batteries determined with adiabatic calorimetry methodology. Applied Energy, 100, 127 (2012).
5. C.-Y. Jhu, Y.-W. Wang, C.-M. Shu, J.-C. Chang, H.-C. Wu, Thermal explosion hazards on 18650 lithium ion batteries with a VSP2 adiabatic calorimeter. Journal of Hazardous Materials, 192, 99 (2011).

Preprints (www.preprints.org) | NOT PEER-REVIEWED | Posted: 10 February 2017 doi:10.20944/preprints201702.0033.v1

Peer-reviewed version available at *Batteries* **2017**, *3*, , 14; doi:10.3390/batteries3020014

6. W. C. Chen, Y. W. Wang, C. M. Shu, Adiabatic calorimetry test of the reaction kinetics and self-heating model for 18650 Li-ion cells in various states of charge. J. Power Sources, 318, 200 (2016).
7. M. Fleischhammer, T. Waldmann, G. Bisle, B-I. Hogg, M. Wohlfahrt-Mehrens, Interaction of cyclic ageing at high-rate and low temperatures and safety in lithium-ion batteries. J. Power Sources, 274, 432 (2015).
8. T. Lu, C. Chiang, S. Wu, K. Chen, S. Lin, C. Wen, C. Shu, Thermal hazard evaluations of 18650 lithium-ion batteries by an adiabatic calorimeter. J Therm Anal Calorim, 114, 1083 (2013).
9. O. Mendoza-Hernandez, H. Ishikawa, Y. Nishikawa, Y. Maruyama, M. Umeda, Cathode material comparison of thermal runaway behavior of Li-ion cells at different state of charges including over charge. J. Power Sources, 280, 499 (2015).
10. C. Orendorff, J. Lamb, L. A. Steele, S. W. Spangler, J. Langendorf, Quantification of Lithium-ion Cell Thermal Runaway Energetics. SANDIA REPORT, SAND2016-0486, January 2016.
11. J. R. Selman, S. A. Hallaj, I. Uchida, Y. Hirano, Cooperative research on safety fundamentals of lithium batteries. J. Power Sources, 97-98, 726 (2001).
12. A. W. Golubkov, D. Fuchs, J. Wagner, H. Wiltsche, C. Stangl, G. Fauler, G. Voitic, A. Thaler, V. Hacker, Thermal-runaway experiments on consumer Li-ion batteries with metal-oxide and olivin-type cathodes. Journal of RSC Advances, 4, 3633 (2014).
13. Malgorzata K. Gulbinska. Lithium-ion Battery Materials and EngineeringEditors, p 3, Springer, London (2014).
14. H. F. Xiang, H. Wang, C. H. Chen, X. W. Ge, S. Guo, J. H. Sun, W. Q. Hu, Thermal stability of LiPF6-based electrolyte and effect of contact with various delithiated cathodes of Li-ion batteries. J. Power Sources, 191, 575 (2009).
15. E. Schuster, C. Ziebert, A. Melcher, M. Rohde, H.J. Seifert, Thermal behavior and electrochemical heat generation in a commercial 40 Ah lithium ion pouch cell Journal of Power Sources, 286, 580 (2015).
16. A. Melcher, C. Ziebert, M. Rohde, H.J. Seifert, Modeling and Simulation of the Thermal Runaway Behavior of Cylindrical Li-Ion Cells—Computing of Critical Parameters. Energies, 9 292 (2016), doi:10.3390/en9040292.
17. J. Newman, W. Tiedemann, Temperature Rise in a Battery Module with Constant Heat Generation. J. Electrochem. Soc., 142, 1054 (1995).

© 2017 by the authors; licensee *Preprints*, Basel, Switzerland. This article is an open access article distributed under the terms and conditions of the Creative Commons by Attribution (CC-BY) license (http://creativecommons.org/licenses/by/4.0/).